Deviation from Corresponding States for a Fluid of Square Well Spherocylinders

Dave C. Williamson* and Yolanda Guevara

Instituto de Física, Universidad de Guanajuato, Apdo Postal E-143, León, Guanajuato, 37150 México

Received: February 1, 1999; In Final Form: May 20, 1999

The nonconformal behavior of a fluid of hard spherocylinders with a spherocylindrical square well attraction is examined using a simple perturbation theory in which the thermodynamics of the anisotropic fluid is mapped to that of an equivalent spherical system. This theory was shown to give a good description of the thermodynamic properties of the isotropic phase of a fluid of hard core aspect ratio 5:1 and square well range $\lambda = 1.5$. To date no simulation data exists for the vapor−liquid region of this model; however, the theoretical predictions are compared with Gibbs ensemble Monte Carlo simulation data for the linear Kihara potentials. A strong similarity is observed. in the phase behavior of both fluids. The square well system has the advantage that there is a good theoretical equation of state in which the range parameter can be varied without extra computational difficulty. Finally, despite the simplicity of the square well model, we demonstrate that this model can be used to describe the vapor−liquid coexistence of the alkane chain series from ethane to octane.

1. Introduction

The evaluation of the thermodynamic properties of fluids of nonspherical molecules from statistical mechanics has received a good deal of attention during the past 20 years.[1] Special emphasis has been placed on understanding the role played by molecular anisotropy on deviation from the principle of corresponding states. This work can be split into two groups: anisotropy introduced through molecular shape (see refs 2, 3 and the references therein) and those where the anisotropy is introduced through multipolar forces. In fact there are even studies which included both shape anisotropy and multipolar anisotropy in the same model. In this work we concentrate on the role played by anisotropy in the molecular shape. The attention of the reader interested in work on polar fluids is drawn to the following recent studies refs 4−7 and references therein).

In the study of fluids, perturbation theories (PT) have proved themselves to be extremely useful tools for the evaluation of thermodynamic properties. Over the last 15 years several perturbation theories have appeared which describe the thermodynamics, with varying degrees of success, of a variety of models which include nonsphericity in the molecular shape. These models include the site−site potentials (see references 1−8 of ref 9), the nonspherical Kihara potentials[8] and the Berne−Pechukas type potentials based on the Gaussian overlap model.[10] The Gay−Berne potential should also be included here;[9] however, it is a more complex potential with a shifted Lennard−Jones form and an anisotropic potential well depth and the perturbation theories, e.g., ref 11, for this family of potentials are more scarce and much less accurate than the best PT for the simpler models.

Of particular relevance to this work are the studies of the linear Kihara (LK) models,[8] since this family of potentials could be considered as having a repulsive core with spherocylindrical geometry. Historically the first PT for the Kihara potentials was developed by Boublík[12] in the mid-seventies. More recently, Vega and Lago proposed a second order PT base on the RAM theory.[13] The results of this theory showed sizable but systematic deviations from simulation data in the first order perturbation term at high densities and large elongations. The theory was corrected using the simulation data and the subsequent results from the improved theory were found to give good agreement with Gibbs ensemble Monte Carlo simulation results for the liquid−vapor (LV) coexistence region. The theoretical results in conjunction with the simulation data were used to illustrate the role of molecular elongation on nonconformal behavior.[2] In addition to these studies, Boublík[14] has also presented a detailed examination of the critical properties of the linear Kihara model.

Recently, the square well analogue of the linear Kihara potential, the square well spherocylinder (SWSC), was proposed as a simple model nematogen which included attractive interactions.[15] The SW potential was chosen since in its spherical form it has been used with a great deal of success to model nonpolar spherical fluids and the simplicity of the SW interaction leads to a closed form equation of state without any corrections requiring simulation data. A second virial coefficient resummation was proposed to descibe the thermodynamics of the isotropic−nematic (IN) phase transition. The predictions obtained from the theoretical equation of state were found to be in good agreement with simulation data for the isotropic phase up to densities close to the IN phase transition. Using this equation of state (EOS) the deviation from correponding states is examined as a function of molecular shape anisotropy for a range of anisotropies roughly equal to those of nitrogen and carbon dioxide upto those equivalent to heptane and octane.

This paper is divided as follows. In the following section we give a description of the theoretical procedure. In section 3 we discuss the general effects of elongation of the liquid−vapor coexistence region comparing with the results for the linear Kihara fluids. In section 4 we use the SWSC fluid to model the thermodynamic properties of the *n*-alkanes from ethane to octane. Finally in section 5 we draw our conclusions.

2. Theory

Let us consider a system of N molecules in a volume V at a temperature T. The number density ρ is defined as N/V. The coordinates of the center of mass of a molecule i are written as $\mathbf{r}_i$ and the orientational coordinates as Ω_i. The orientational

10.1021/jp990353o CCC: $18.00
Published on Web 08/13/1999

coordinates are considered normalized as

$$\int d\Omega_i = 1 \tag{1}$$

In the case of a linear molecule $d\Omega_i$ may be written as $d\cos\theta d\phi/4\pi$, where θ is the polar angle of the molecular axis and ϕ the azimuthal angle. The full set of translational and orientational coordinates will be written as $d\mathbf{i} = d\mathbf{r}_i d\Omega_i$.

The compressibility factor Z can be written in terms of a power series of the packing fraction $\eta = \rho\nu_m$, where ν_m is the volume of a molecule

$$Z = 1 + \sum_{n=2}^{\infty} B_n^* \eta^{n-1} \tag{2}$$

Here $B_n^* = B_n/\nu_m^{n-1}$, is the reduced nth virial coefficient. Providing the virial series converges the excess Helmholtz free energy is given by

$$\frac{A^{\text{excess}}}{NkT} = \int \frac{Z-1}{\eta} d\eta \tag{3}$$

and using expression 2 by

$$\frac{A^{\text{excess}}}{NkT} = \sum_{n=2}^{\infty} \frac{B_n^* \eta^{n-1}}{(n-1)} \tag{4}$$

In perturbation theory the potential is separated into two parts

$$U = U_o + \alpha U_p(\mathbf{1},\mathbf{2}) \tag{5}$$

where $U_o(\mathbf{1},\mathbf{2})$ is a reference potential and $U_p(\mathbf{1},\mathbf{2})$ is the perturbing potential. The parameter α varies between 0 and 1 and allows the perturbation potential to be switched on.

With the ideas of PT in mind it is possible to consider a similar division of the virial coefficients

$$B_n = B_n^{\text{rep}} + B_n^{\text{att}} \tag{6}$$

For the second virial coefficient this would be

$$B_2^{\text{rep}} = -\frac{1}{2}\int\int\int\int_o^{r_c} (\exp(-\beta U_o) - 1) \times r_{12}^2\, dr_{12} d\hat{\mathbf{r}}_{12} f(\mathbf{\Omega_1}) f(\mathbf{\Omega_2}) d\mathbf{\Omega_1} d\mathbf{\Omega_2} \tag{7}$$

and

$$B_2^{\text{att}} = -\frac{1}{2}\int\int\int\int_{r_c}^{\infty} (\exp(-\beta U_p(\mathbf{12})) - 1) \times r_{12}^2\, dr_{12} d\hat{\mathbf{r}}_{12} f(\mathbf{\Omega_1}) f(\mathbf{\Omega_2}) d\mathbf{\Omega_1} d\mathbf{\Omega_2} \tag{8}$$

where r_c is the edge of the hard core. It is clear from the expressions above that the second virial coefficient can be neatly divided into a contribution which depends only on the repulsive potential and a contribution which depends only on the attractive potential. In the case of the higher virial coefficients, the division into a repulsive contribution and attractive contribution requires a little more care. In order to illustrate this, the case of the third virial coefficient will be considered. Defining

$$f(ij) = \exp(-\beta U) - 1 \tag{9}$$

$$f_o(ij) = \exp(-\beta U_o) - 1 \tag{10}$$

and

$$f_p(ij) = \exp(-\beta U_p(\mathbf{12})) - 1 \tag{11}$$

we can write the third virial coefficient as

$$B_3 = -\frac{1}{3}\int\int\int\int\int\int f(12) f(13) f(23) \times d(\mathbf{r_{12}}) d(\mathbf{r_{13}}) f(\mathbf{\Omega_1}) f(\mathbf{\Omega_2}) f(\mathbf{\Omega_3}) d\mathbf{\Omega_1} d\mathbf{\Omega_2} d\mathbf{\Omega_3} \tag{12}$$

The repulsive part of the third virial coefficient is defined when all three molecules simultaneously overlap, i.e.,

$$B_3^{\text{rep}} = -\frac{1}{3}\int\int\int\int\int\int_o^{r_c}\int_o^{r_c} f_o(12) f_o(13) f_o(23) \times r_{12}^2\, dr_{12} r_{13}^2\, dr_{13} d\hat{\mathbf{r}}_{12} d\hat{\mathbf{r}}_{13} f(\mathbf{\Omega_1}) f(\mathbf{\Omega_2}) f(\mathbf{\Omega_3}) d\mathbf{\Omega_1} d\mathbf{\Omega_2} d\mathbf{\Omega_3} \tag{13}$$

The attractive contribution to the third virial coefficient can now be defined as

$$B_3^{\text{att}} = B_3 - B_3^{\text{rep}} \tag{14}$$

This means that the integral necessary to calculate B_3^{att} involves terms with integrands of the form $f_p(12)f_p(13)f_p(23)$, $f_o(12)f_p(13)f_p(23)$, and $f_o(12)f_o(13)f_p(23)$, and all the possible permutations. The same is true for the higher virial coefficients.

Substituting expression 6 into 4

$$\frac{A_{\text{iso}}^{\text{excess}}}{NkT} = \sum_{n=2}^{\infty}\left(\frac{B_n^{*\text{rep}}}{(n-1)} + \frac{B_n^{*\text{att}}}{(n-1)}\right)\eta^{n-1} \tag{15}$$

Hence, for the isotropic phase the excess free energy can be seperated into the repulsive contribution and the attractive contribution

$$\frac{A_{\text{iso}}^{\text{excess}}}{NkT} = \frac{A^{\text{rep}}}{NkT} + \frac{A^{\text{att}}}{NkT} \tag{16}$$

where

$$\frac{A_{\text{iso}}^{\text{rep}}}{NkT} = \sum_{n=2}^{\infty}\frac{B_n^{*\text{rep}}}{(n-1)}\eta^{n-1} \tag{17}$$

and

$$\frac{A_{\text{iso}}^{\text{att}}}{NkT} = \sum_{n=2}^{\infty}\frac{B_n^{*\text{att}}}{(n-1)}\eta^{n-1} \tag{18}$$

The model potential comprises a spherocylindrical hard core, defined by L^* (the ratio of the cylinder length L to diameter D), with a spherocylindrically shaped square well attraction of range λD. Here $(\lambda - 1)D/2$ is the distance from the edge of the repulsive core to the edge of the square well sheath. The potential is defined as

$$U(\mathbf{r_{ij}},\mathbf{\Omega_i},\mathbf{\Omega_j}) = \begin{cases} \infty, & r_{ij} \in V_{ex}(\mathbf{\Omega_i},\mathbf{\Omega_j}) \\ -\epsilon, & s_{ij}(\mathbf{r_{ij}},\mathbf{\Omega_i},\mathbf{\Omega_j}) \le \lambda D \\ 0, & s_{ij}(\mathbf{r_{ij}},\mathbf{\Omega_i},\mathbf{\Omega_j}) > \lambda D \end{cases}$$

where ϵ is the square well depth and $s_{ij}(\mathbf{r_{ij}},\mathbf{\Omega_i},\mathbf{\Omega_j})$ is the closest approach between two line segments.

The repulsive and attractive contributions to the second virial coefficient for this model are

$$B_2^{\text{rep}} = \frac{1}{2}\int\int V_{\text{exc}}(\mathbf{\Omega_1},\mathbf{\Omega_2}) f(\mathbf{\Omega_1}) f(\mathbf{\Omega_2}) d\mathbf{\Omega_1} d\mathbf{\Omega_2}$$

$$B_2^{\text{att}} = \left[\frac{1}{2}\int\int V_{\lambda}(\mathbf{\Omega_1},\mathbf{\Omega_2}) f(\mathbf{\Omega_1}) f(\mathbf{\Omega_2}) d\mathbf{\Omega_1} d\mathbf{\Omega_2}\right]\left[\exp\left(\frac{1}{T^*}\right) - 1\right] \tag{19}$$

where

$$V_{\text{exc}}(\mathbf{\Omega_1},\mathbf{\Omega_2}) = \frac{4\pi D^3}{3} + \frac{\pi L D^2}{2} + 2L^2 D \sin\gamma$$

$$V_{\lambda}(\mathbf{\Omega_1},\mathbf{\Omega_2}) = \frac{4\pi(\lambda^3 - 1)D^3}{3} + \frac{\pi(\lambda^2 - 1)LD^2}{2} + 2(\lambda - 1)L^2 D \sin\gamma \tag{20}$$

Here, γ is the angle between the molecular vectors of particles 1 and 2 and $T^* = kT/\epsilon$. In the isotropic phase $f(\mathbf{\Omega})$ is uniform such that using eq 1 we find that $f(\mathbf{\Omega}) = 1$. Substituting eq 14 into eq 13 allows us to perform the integrals over the molecular orientations yielding expressions for the isotropic second virial coefficient

$$B_2^{\text{rep}}(iso) = \frac{2\pi D^3}{3} + \pi L D^2 + \frac{\pi L^2 D}{4}$$

$$B_2^{\text{att}}(iso) = \left[\frac{2\pi(\lambda^3 - 1)D^3}{3} + \pi(\lambda^2 - 1)LD^2 + \frac{(\lambda - 1)\pi L^2 D}{4}\right]\left[\exp\left(\frac{1}{T^*}\right) - 1\right] \tag{21}$$

In order to construct an approximate expression for the excess free energy of the isotropic phase of SWSC fluid we will use the fact that for perfectly aligned hard convex bodies (HCB) the reduced virial coefficients B_n^* are equal to the reduced virial coefficients of an equivalent hard sphere (HS) system

$$B_n^{*\|}(\text{HCB}) = B_n^*(\text{HS}) \tag{22}$$

This assumption is exact for parallel hard ellipsoids and for the second virial coefficient of the hard spherocylinder fluid; however, for the higher virial coefficients of the hard spherocylinder fluid this is an approximation.[16] In essence this main assumption, necessary to obtain the EOS for parallel SWSC, is to consider the fluid to be behaving as a fluid of spherical SW molecules with equivalent hard core volumes. Equating hard core volumes we have

$$\frac{\pi D_{\text{eff}}^3}{6} = \frac{\pi D^3}{12}(2 + 3L^*) \tag{23}$$

which leads to

$$\frac{D_{\text{eff}}^3}{D^3} = 1 + \frac{3L^*}{2} \tag{24}$$

where D_{eff} is the diameter of the effective spherical hard core. In order to calculate the effective SW range of the reference spherical fluid we must equate the "volumes" of the SW region of the sperocylindrical model and the effective spherical reference, which gives us

$$\frac{\pi D_{\text{eff}}^3}{6}(\lambda_{\text{eff}}^3 - 1) = \frac{\pi D^3}{12}(2(\lambda^3 - 1) + 3L^*(\lambda^2 - 1)) \tag{25}$$

Rearranging eq 19 and using eq 18, the effective square well range λ_{eff} can be calculated from the expression

$$\lambda_{\text{eff}}^3 = \frac{2^*\lambda^3 + 3L^*\lambda^2}{2 + 3L^*} \tag{26}$$

Using the spherical SW as a reference and making the approximation

$$B_n = \frac{B_n^{\|} B_2}{B_2^{\|}} \tag{27}$$

which allows us to map the thermodynamics of the SWSC fluid to those of a spherical square well the excess free energy of the isotropic SWSC fluid can be written as

$$\frac{A_{\text{iso}}^{\text{excess}}(\text{SWSC})}{NkT} = \frac{B_2^{\text{rep}}}{B_2^{\text{rep}\|}}\left(\frac{A^{\text{excess}}(\text{HS})}{NkT}\right) + \frac{B_2^{\text{att}}}{B_2^{\text{att}\|}}\left(\frac{A^{\text{excess}}(\text{SW})}{NkT}\right) \tag{28}$$

where

$$B_2^{\text{rep}\|}(\text{iso}) = \frac{2\pi D^3}{3} + \pi L D^2$$

$$B_2^{\text{att}\|}(\text{iso}) = \left[\frac{2\pi(\lambda^3 - 1)D^3}{3} + \pi(\lambda^2 - 1)LD^2\right]\left[\exp\left(\frac{1}{T^*}\right) - 1\right]$$

The attractive part of free energy of the spherical square well is calculated from the expression derived by Gil-Villegas et al.,[17] while the repulsive part is calculated from the expression of Carnahan and Starling.[18] It should be noted that in this case the repulsive contribution to the free energy is identical to the expression derived by Lee[19] from the original work of Parsons.[20] This expression has been shown to give an excellent description of the thermodynamic properties of several fluids consisting of hard convex bodies.

3. Results

In a recent paper[15] the accuracy of the equation of state presented here was tested against simulation data for a SWSC fluid with hard core anisotropy, $L/D = 5$, and SW range $\lambda = 1.5$. The theoretical predictions for the thermodynamic properties were found to be in good agreement with the simulation data for densities ranging from ideal gas values to values close to the IN phase transition. In fact, results for the thermodynamic properties at the phase transition were also found to be in good agreement.

In this work we present results for the LV coexistence for SWSC fluids of much smaller elongations. Since the theory involves mapping the thermodynamics of the SWSC fluid to those of an effective spherical SW fluid, it is assumed that, away from the critical point, the results will be of, at least, the same accuracy those for the 5:1 system.

To begin with, the general effects that various molecular parameters have on the critical properties and the deviation from corresponding states behavior are presented. However, it should be noted that only the general trends for the critical properties

TABLE 1: Theoretical Predictions for the Critical Properties and Acentric Factor ω for SWSC with L/D Ranging from 0.0 to 3.0 and Fixed SW Range $\lambda = 1.5$

L/D	T_c^*	P_c^*	ρ_c^*	η_c	ω
0.0	1.412	0.1975	0.3153	0.1651	−0.1615
0.1	1.363	0.1721	0.2811	0.1693	−0.1541
0.2	1.322	0.1525	0.2534	0.1725	−0.1442
0.3	1.285	0.1359	0.2310	−0.1754	−0.1370
0.4	1.253	0.1226	0.2120	0.1776	−0.1248
0.5	1.225	0.1117	0.1956	0.1792	−0.1133
0.6	1.199	0.1021	0.1817	0.1808	−0.1032
0.7	1.175	0.0937	0.1697	0.1821	−0.0912
0.8	1.154	0.0868	0.1588	0.1829	−0.0835
0.9	1.134	0.0805	0.1494	0.1838	−0.0726
1.0	1.116	0.0751	0.1408	0.1843	−0.0606
1.2	1.083	0.0659	0.1264	0.1853	−0.0390
1.5	1.041	0.0553	0.1094	0.1862	−0.0035
2.0	0.985	0.0431	0.0890	0.1864	0.0508
3.0	0.906	0.0291	0.0642	0.1849	0.1559

can be taken. The reason for this is that perturbation theories of the kind used here systematically overestimate the critical properties since the region of the LV envelope close to the critical point, as described by the perturbation theory, takes a classical, parabolic form.

In Table 1 the theoretical critical properties (T_c^*, P_c^*, ρ_c^*, and η_c^*) are presented for the SWSC fluid with several different elongations at fixed SW range, $\lambda = 1.5$. Clearly the effect of molecular elongation is to reduce the critical temperature. This result suggests that, for fixed SW range, as the core length is increased the overall pair interaction becomes more repulsive. This can be seen when the potential is sphericalized, as described in the previous section, and when the effective SW range is calculated, according to expression 26, we find that the λ_{eff} decreases with increased elongation. As the molecular elongation is increased a decrease in the critical density is observed. Clearly as the molecular anisotropy is increased the molecular volume is increasing and this effect accounts, to some extent, for the decrease in the critical density. However, when the critical packing fraction is examined it should be noted that the decrease in critical density is smaller than the accompanying increase in molecular volume, thus we observe an increase in the critical packing fraction.

As the temperature is lowered the attractive interactions give a larger negative contribution to the pressure. From these observation we propose that despite the fact that the critical packing fraction is increasing and the overall effect of molecular elongation is to increase the repulsive character of the intermolecular potential, the critical pressure decreases because the critical temperature has also decreased. In fact, data obtained from both computer simulation and perturbation theory also show the same trends[2] for the linear Kihara (LK) fluids. Later in this section the similarities and differences between the SWSC and the LK fluids are discussed.

In Figure 1 the liquid−vapor coexistence curves for SWSC fluids with $\lambda = 1.5$ and elongations of $L/D = 0$, 0.3, 0.6, 0.8, 1.2 are presented. As mentioned above we can see the decrease in critical temperature and critical density which are accompanied by a narrowing of the biphasic region as the molecular elongation is increased. In Figure 2 the dependence of the vapor pressure on temperature is presented as Clausius−Clapeyron plots for the same systems. The results clearly show a linear dependence, as has been observed experimentally for many systems and also from simulation data for the linear Kihara molecules. What is far more striking is the fact that the results for different elongations with fixed λ are almost parallel to each other.

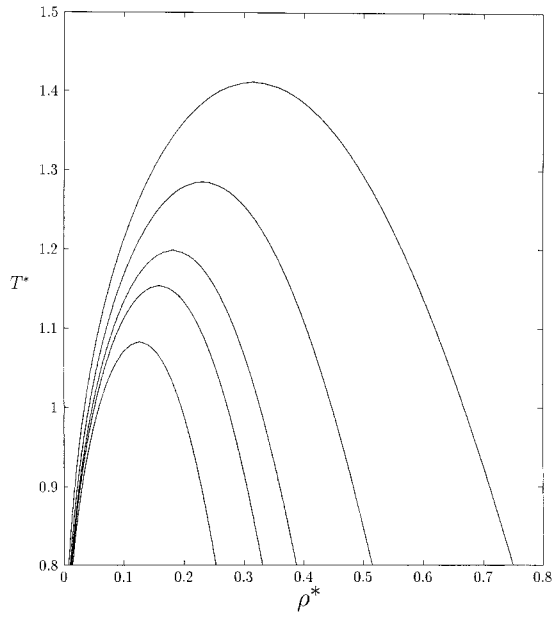

Figure 1. The $T^* - \rho^*$ plot for the LV coexistence of SWSC fluids with fixed SW range $\lambda = 1.5$. The curves correspond to hard core aspect ratios $L/D = 0.0$, 0.3, 0.6, 0.8, 1.2. Where the orthobaric with the highest critical temperature corresponds to the spherical SW fluid $L/D = 0.0$, and the curve with the lowest critical temperature corresponds to the system with $L/D = 1.2$. The second, third, and fourth curves in order of decreasing critical temperature correspond to the systems with $L/D = 0.3$, 0.6, 0.8, respectively.

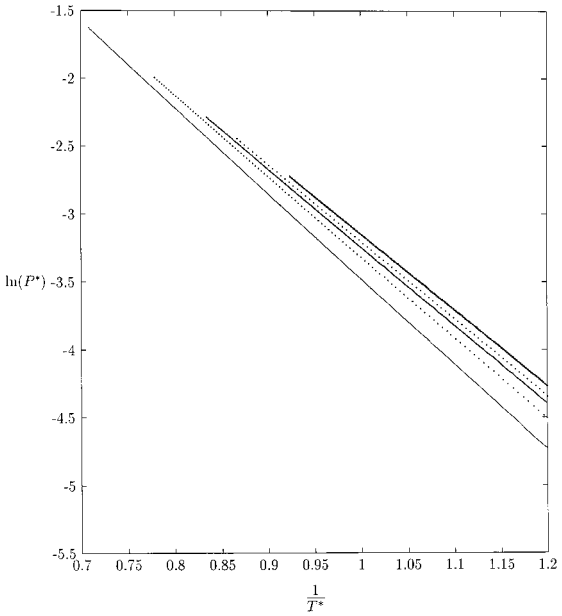

Figure 2. The Clausius−Clapeyron plots for SWSC fluids with fixed SW range, $\lambda = 1.5$, and increasing anisotropy, $L/D = 0.0$, 0.3, 0.6, 0.8, 1.2. The lower bold line corresponds to the data for the spherical SW fluid, $L/D = 0.0$. The anisotropic fluids, $L/D = 0.3$, 0.6, 0.8, 1.2, are represented by the subsequent lines, the lowest (bold dotted) corresponding to the $L/D = 0.3$ fluid to the upper line which represents the $L/D = 1.2$ fluid.

As observed from the results above and from the study of the linear Kihara fluids,[2] molecular anisotropy has a non-negligible effect on critical properties and liquid−vapor phase coexistence. It has been demonstrated,[21] however, that when the coexistence properties are reduced with the appropriate critical values, a great number of real fluids show, to a close approximation, the same behavior. This correlation is known as the law of corresponding states. Several molecules with

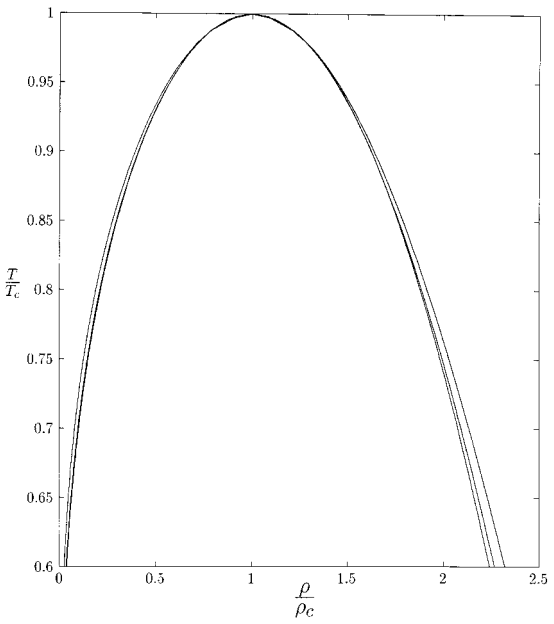

Figure 3. The LV coexisting densities plotted in units reduced with the critical values for the SWSC fluids with fixed SW range, $\lambda = 1.5$ and elongations, $L/D = 0.0, 0.3, 1.2$. On the liquid branch the outermost line corresponds to the spherical SW fluid, the middle line to elongation $L/D = 0.3$, and the innermost line to the fluid with elongation $L/D = 1.2$. For the vapor branch the spherical fluid and the shorter elongated fluid, $L/D = 0.3$, are virtually indistinguishable, while the outer line corresponds to the fluid with elongation $L/D = 1.2$.

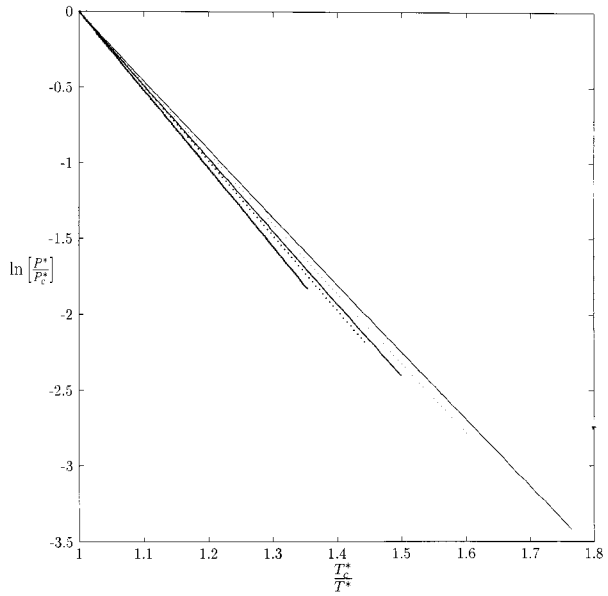

Figure 4. The Clausius−Clapeyron plots, in units reduced by the corresponding critical values, for SWSC fluids with fixed SW range, $\lambda = 1.5$, and increasing anisotropy, $L/D = 0.0, 0.3, 0.6, 0.8, 1.2$. The upper line corresponds to the data for the spherical SW fluid, $L/D = 0.0$. The anisotropic fluids, $L/D = 0.3, 0.6, 0.8, 1.2$, are represented by the subsequent lines, the first (dotted) corresponding to the $L/D = 0.3$ fluid to the lowest line which represents the $L/D = 1.2$ fluid.

spherical or almost spherical symmetry have been found to obey the law of corresponding states. Most notably the Noble gases conform very well, and even oxygen and nitrogen show a strong similarity to corresponding state behavior.

For intermolecular potentials of spherical symmetry, we may reduce the potential using two parameters, one is an energy scale and the second a length scale. The reduced thermodynamic properties can be calculated for the potential, and the results represent a possible family of substances which differ only in the length and energy scale. At the level of intermolecular potentials, this is the manifestation of the principle of corresponding states. For many substances which are strongly polar and/or highly nonspherical, we often encounter strong deviations from corresponding state behavior. Pitzer[22] observed that in order to describe nonconformal behavior, a third parameter is required which allows us to descibe a family of potentials. A good example for spherical potentials is the Mie $m-n$ potentials of which the Lennard−Jones potential is a member. Other possibilities are the inclusion of molecular polarity or, as in this case, the inclusion of anisotopy. It is, therefore, useful to examine the properties of the liquid−vapor coexistence in terms of the reduced properties.

In Figure 3 the orthobaric curves for the systems $\lambda = 1.5$, $L/D = 0.0, 0.3, 1.2$ are presented in reduced units. In Figure 1 we observed a narrowing of the biphasic region; however, in reduced units we see a shift of both branches of the LV envelope to lower densities. The effect on the vapor branch is almost negligible when the elongation changes from 0.0 to 0.3; however, it is quite marked for the increase in elongation from 0.3 to 1.2. For the liquid branch the nonconformal change is more obvious when the elongation is increased from 0.0 to 0.3 than for the increase 0.3 to 1.2. This result is somewhat strange since real fluids and also the Kihara fluids show a broadening of the liquid coexistence densities as elongation is increased. Whether the results can be attributed to special behavior of the SWSC due to the fixed ranged, the effect of which in comparison to the linear Kihara fluid is discussed below, or is, in fact, a failure of the theory cannot be determined at present. It seems reasonable to suppose that this question will be resolved only in the light of extensive simulation data for the LV phase behavior.

The nonconformal behavior in the Clausius−Clapeyron plots are presented in Figure 4. We can see that the slope of the Clausius−Clapeyron plot is negative and increases with elongation. The nonconformal behavior of the Clausius−Clapeyron plot can be described using Pitzer's acentric factor

$$\omega = -\log_{10}(P_r) - 1 \qquad (30)$$

where P_r is the reduced pressure calculated at $T_r = 0.7$. The acentric factors are given in Table 1 for elongations from 0 to 3. The acentric factor, which is related to the slope of the Clausius−Clapeyron plot, is found to increase with increasing elongation. In Figure 5 the acentric factor is presented as a function of elongation; the points are the values of ω calculated from the theory and the line is a straight line fit through the data. It is interesting to note that over the range of elongations presented here, the plot is virtually linear. This lends a certain amount of support to Pitzer's idea that the thermodynamics of a nonconformal family of substances might be described using some kind of thermodynamic expansion in the acentric factor.

Almost all of the general trends observed above are also observed for the linear Kihara fluids. In Figure 6 a direct comparison of the orthobarics (in units of σ and ϵ) of three SWSC and the Gibbs ensemble simulation data for linear Kihara molecules with elongations 0.3, 0.6, 0.8 are presented. The results for the SWSC are compared with simulation data for the LK fluids mainly to demonstrate the similarities between the two models; however, since no simulation data exists for the SWSC in the region of the LV phase transition it also gives a rough idea of whether or not the theory is producing sensible results. The three SWSC systems were chosen to have the same

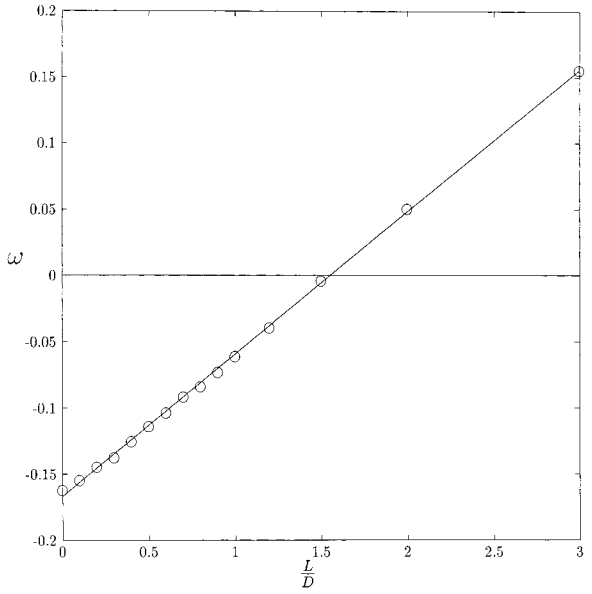

Figure 5. The acentric factor (ω) plotted as a function of aspect ratio (L/D) for the SWSC fluid with fixed SW range, $\lambda = 1.5$. The points represent the data values from Table 1, and the line is a best fit straight line through the data.

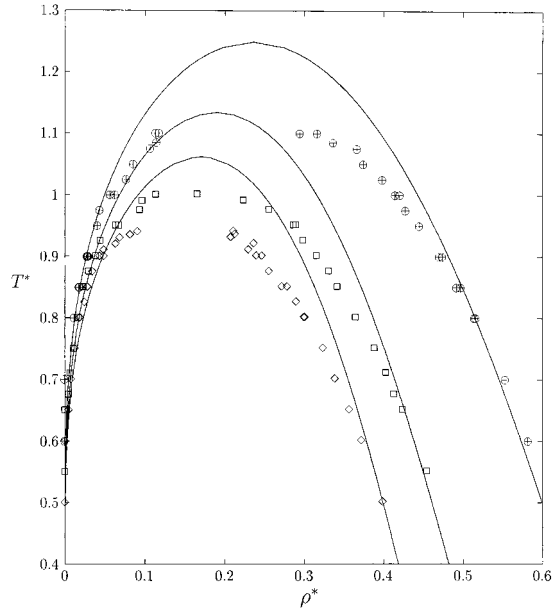

Figure 6. LV coexistence curves for SWSC and Gibbs ensemble Monte Carlo simulation data for three linear Kihara fluids. The points represent the simulation data for fluids of linear Kihara molecules with elongations, 0.3 (circles with crosses), 0.6 (open squares), and 0.8 (open diamonds). The lines correspond to theoretical predictions for fluids of SWSC molecules with $\lambda = 1.48$, $L/D = 0.3$ (upper curve); $\lambda = 1.46$, $L/D = 0.6$ (middle curve); and $\lambda = 1.44$, $L/D = 0.8$ (lower curve).

elongation as their Kihara counterpart, and λ was chosen to give the best fit for the orthobaric curves. The agreement between the theory and simulation results is surprisingly good. The difference between the simulation data and the theoretical results can be explained in terms of the LK having a soft repusive core. Clearly the shape and size of the hard core in the SWSC model is well defined by the aspect ratio, L/D. In the case of the LK, however, if we consider the traditional Barker−Henderson (BH) repulsive core, we find that it will vary with temperature since the diameter of the repulsive core will be equal to the BH diameter $\delta(T)$ for the Lennard−Jones potential. Thus the effective core aspect ratio would be $L^*/\delta(T)$, where L^* is the length of the LK line segment in units of σ. Better comparison between the two models could be obtained using this type of mapping; however, it is not the purpose of this paper to attempt such a detailed comparison.

An interesting feature of the comparsion presented here is the fact that in order to describe the LV envelope in a reasonable manner the SW range must be decreased as the molecules are elongated. In some way this is compensation for the fact that the hard core aspect ratio is not temperature dependent; however, it also suggests a greater increase in the repulsive character of the LK molecule with increasing elongation that is found in the SWSC model. Clearly the LK and SWSC fluid share similar phase behavior and either is a viable model for the study of nonconformal behavior in nonspherical, nonpolar fluids.

4. Fitting to *n*-Alkanes

So far we have used the SWSC model to examine the general effects of molecular elongation on LV phase behavior. It is also interesting to see whether such a simple model contains sufficient physical information to describe the LV phase behavior of real substances. We choose the *n*-alkane series to test our model for several reasons. First, there is a good deal of reliable experimental data for the *n*-alkane series from methane to octane. Second, the alkanes have virtually no polar character so it should be possible to describe, to a certain extent, the nonconformal behavior of the series through molecular elongation. Third, the *n*-alkane series was recently modeled with a chain of spherical SW segments whose thermodynamics were calculated using the SAFT-VR equation of state.[3] It is interesting to discover how a simple model such as the SWSC compares with a more sophisticated model.

The theoretical results were fitted to the experimental data using the method described by Guevara et al.[7] An experimental point is chosen corresponding to a reduced temperature of approximately $T_r = 0.6$. We then take the liquid density ρ_l at this point and the vapor pressure P_v, making a choice for λ and for L^* we obtain the liquid density ρ_l^* and vapor pressure P_v^* for the model system from which we obtain the values of σ and ϵ required to reproduce ρ_l and P_v. The full orthobaric and vapor pressure curves for the model are then reduced with the values of σ and ϵ and compared with the experimental results. New λ and L^* are chosen until the best fit with the experimental data is found. The experimental data used for these fittings were taken from the thermodynamic data tables compiled by Smith and Srivastava.[23] Clearly with four parameters to fit, the fitting process can become time consuming. It would therefore be useful if some parameters were transferable from one alkane to the next, as was the case for the SW chains studied by Gil-Villegas et al. The fitting of the alkane series from ethane to octane is carried out as follows. The best fit to ethane is made first. In this fitting L/D and λ are varied in order to obtain the best fit for λ. The most appropriate value for the SW range was found to be $\lambda = 1.65$. This value is then kept constant when the subsequent fittings are made for the other alkanes. A fitting is then made to the experimental results for propane. In this fitting, L/D is allowed to vary to give the best fit for propane. From this fitting and the fitting for ethane the value for $\Delta L/D$, the increase in the spherocylinder length when the carbon chain is increased by one can be determined. The subsequent fittings are made with λ constant and L/D calculated from $L_{ethane} + (n - 2) * \Delta L/D$ where L_{ethane} is the L/D obtained for ethane and n is the number of carbons in the alkane chain.

The results for the fittings are shown in Table 2. In this table it can be seen that the elongations used to model ethane up to

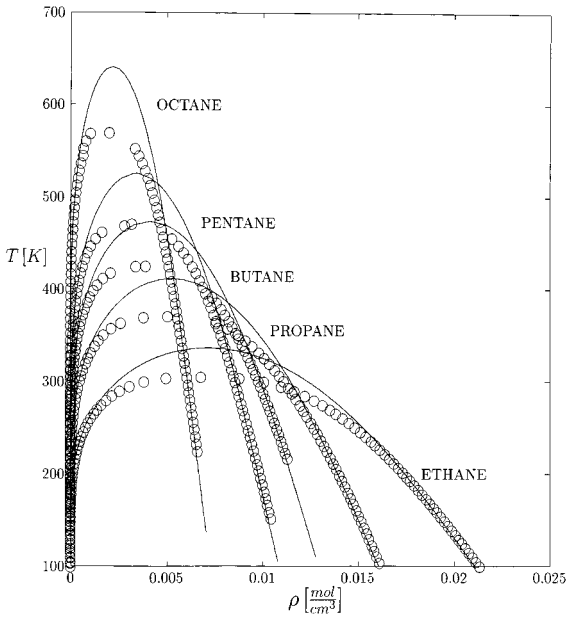

Figure 7. LV coexistence curves for the alkane series. The open circles represent the experimental data and the solid lines represent the fitted theoretical results.

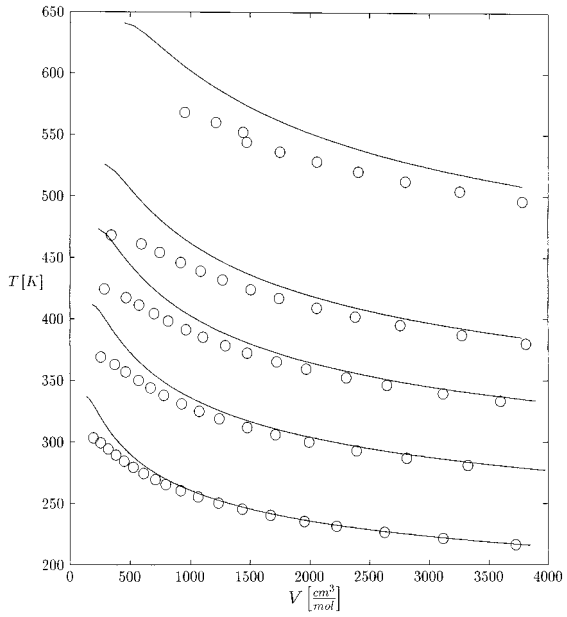

Figure 8. The coexisting vapor volumes for the alkanes ethane (bottom curve), propane, butane, pentane, and octane (top curve). The open circles represent the experimental data and the solid lines represent the fitted theoretical results.

TABLE 2: Fitting Parameters Used to Obtain the Theoretical Descriptions for the LV Coexistence of the Alkane Series Ethane to Octane

C_nH_{2n+2}	L/D	λ	σ[A]	ϵ/k [K]
CH_4	0.0	1.65	3.58	125.90
CH_4	1.8	1.65	2.36	172.10
C_2H_6	2.2	1.65	2.66	291.92
C_3H_8	2.6	1.65	2.79	369.62
C_4H_{10}	3.0	1.65	2.87	438.21
C_5H_{12}	3.4	1.65	2.93	500.52
C_6H_{14}	3.8	1.65	2.96	555.10
C_7H_{16}	4.2	1.65	3.00	605.42
C_8H_{18}	4.6	1.65	3.02	651.52

butane are rather large, when compared to fittings for the LK model.[24] This result merely suggests that in order to achieve the correct balance between repulsive and attractive forces, which results in the correct shape of the orthobaric curve and the Clausius plot, it is not possible to restrict the model parameters to ranges defined by hand-waving arguments about the molecular dimensions of the real system. In other words, the *n*-alkanes are not SWSC nor are they LK molecules; however, their thermodynamic properties can be represented in a satisfactory manner with the appropriate choice of model parameters. To illustrate this point we include results obtained by fitting different SWSC data to methane. In order to avoid possible confusion with the effect of changing the SW range we fix $\lambda = 1.65$ for all of the fittings for methane. Methane is often consider to be a quasispherical molecule, and as such we attempt to fit data for a spherical SW to methane. The fitting parameters are given in Table 2. From Figures 10 and 11 we can see that the fitting is comparable to the fitting obtained for the pure spherical SW in ref 7. However, as can be seen from Table 2, if we are to be consistent with systematic choice of model parameters used for the higher alkanes, we should use an elongation of $L/D = 1.8$ for methane. This fitting is also carried out and the results are collected in Tables 2 and 3. As can be seen from Figures 10 and 11, the fitting using the elongated molecule is somewhat superior to the spherical case. This rather surprising result suggests that, in fact, methane is not very spherical and that a model for methane should include some measure of this nonsphericity. This idea is the basis for

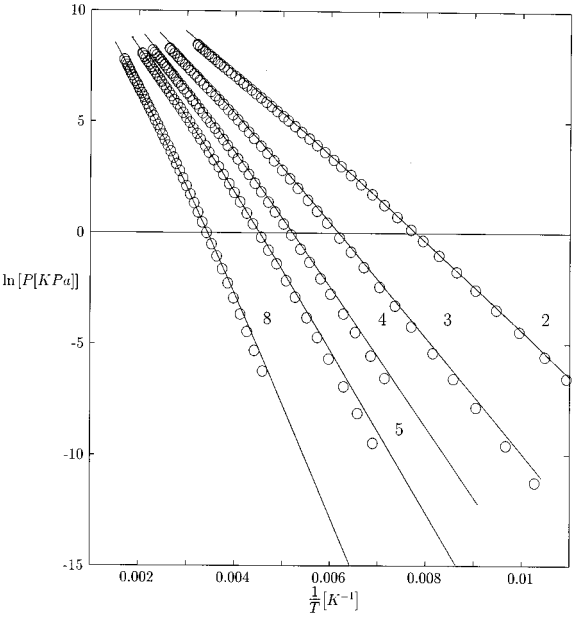

Figure 9. Clausius−Clapeyron plots for ethane, propane, butane, pentane, and octane. The open circles represent the experimental data and the solid lines represent the fitted theoretical results.

the work in reference 7 where the nonsphericity of methane is incorporated using a point octopole. From the results of ref 7 it is clear that the octopolar SW provides the best model for methane.

In the case of the SW chain model, σ was found to increase with increasing chain length, which is what is observed for the SWSC model. However, it appears that in the case of the SWSC model, σ is tending to a limiting value. From Table 2 we also observe that ϵ, the SW depth, increases dramatically as the alkane chain length increases. This can be explained if the alkane is imagined to be a chain of segments, each segment being defined by a carbon atom and its associated hydrogens. In the case of methane we have only one segment, thus the average interaction between two molecules will be equal to the interaction between two segments. As the number of carbons in the

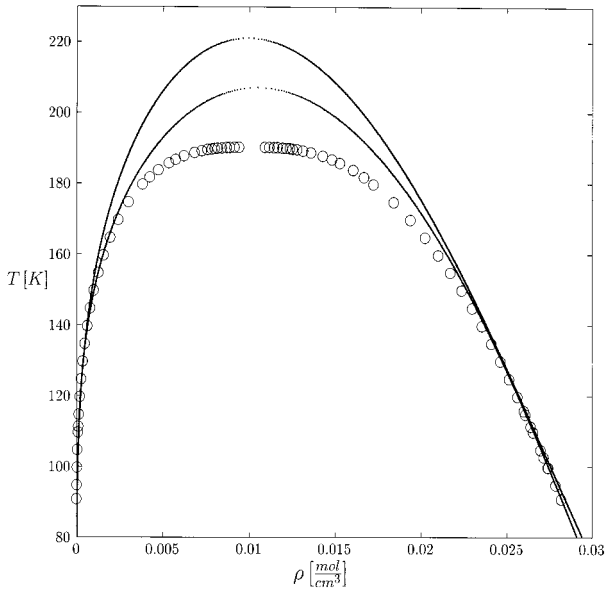

Figure 10. LV coexistence curves for methane. The open circles represent the experimental data and the solid lines represent the fitted theoretical results. The upper solid line, with respect to the critical point, represents the fitting for the spherical SW model ($L/D = 0.0$) and the lower line the fitting for the elongated SWSC model ($L/D = 1.8$).

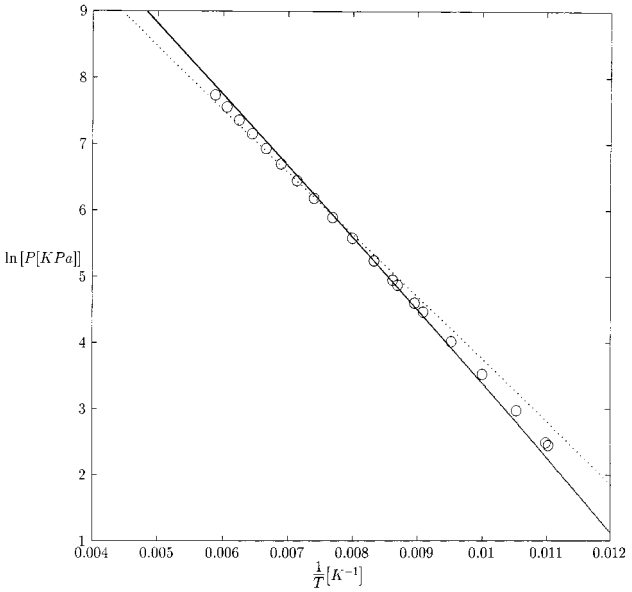

Figure 11. Clausius−Clapeyron plots for methane. The open circles represent the experimental data and the lines represent the fitted theoretical results. The dotted line represents results for the spherical SW model ($L/D = 0.0$) and the solid line results for the elongated SWSC model ($L/D = 1.8$).

alkane chain increases the average number of segment interactions per pair of molecules will increase. If we assume that the segment−segment interaction remains more or less constant from alkane to alkane, we can consider the system to become more attractive as the chain length of the molecules in the system increases. In the SWSC model the number of SW interactions is always 1 for any pair of molecules, thus the increase in the attractive forces, as the alkane chain increases, must be accounted for by increasing the depth of the SW potential. This effect manifests itself when the fittings are made and the value of ϵ in units of k increases with increasing chain length. This rationale is supported, to some extent, by the results obtained for the SW chains. In this model the possible number of SW interactions increases with increasing chain length and, as a result, although ϵ for this model does increase with chain length, the effect is not as marked as for the SWSC model. As mentioned above, the elongations of the models used to fit the alkane data are somewhat larger than those used to fit the alkanes with the LK model. The values of ϵ obtained in this work are found to be smaller than those for the LK fit, and in general the values of σ are also smaller. These trends can be explained in terms of the relative repulsive character of each model. In units reduced by σ and ϵ, highly elongated systems are found to be more repulsive than fluids of shorter molecules. This manifests itself in the lowering of the critical temperature with elongation of the molecules. Thus if a longer molecule is used to fit a data set, the value of ϵ might be expected to be larger to compensate for the stronger repulsive character. On the other hand the LK model becomes more repulsive with elongation than the SWSC, thus we observe a decrease in λ as we elongate the molecules and try and compare the SWSC with the LK. An SW range of $\lambda = 1.65$ more than compensates for the extra repulsive character in the fittings presented in this work, and as such the values of ϵ tend to be smaller for the SWSC than the LK. The differences in the values of σ are also a result of the elongation used. Using the values for σ from Table 2 for methane we can calculate the model molecular volume for the spherical model ($L/D = 0$) and the elongated model ($L/D = 1.8$). In both cases the molecular volume is very similar. Thus a more elongated model for a given alkane will have a smaller value for σ, as is observed. In general though, the trends in σ and ϵ as the alkane chain increases in length are the same for both models.

TABLE 3: Theoretical Predictions for the Critical Properties of the *n*-Alkane Series Methane to Octane

C_nH_{2n+2}	ρ_c [mol/cm^3]	ρ_c [g/cm^3]	T_c [K]	P_c [Mpa]
CH_4 ($L/D = 0$)	0.0099	0.0990	221.08	7.562
CH_4 ($L/D = 1.8$)	0.0104	0.1040	207.04	8.068
C_2H_6	0.007166	0.1290	336.87	9.024
C_3H_8	0.005268	0.1370	411.77	8.156
C_4H_{10}	0.004139	0.1407	473.27	7.386
C_5H_{12}	0.003408	0.1431	525.54	6.774
C_6H_{14}	0.002896	0.1448	569.53	6.261
C_7H_{16}	0.002484	0.1441	607.84	5.746
C_8H_{18}	0.002193	0.1447	641.09	5.340

In Table 3 the theoretical predictions for the critical properties of the *n*-alkane series are presented. From Figures 7 and 9 we can see that, as expected, the critical temperatures and critical pressures are overestimated by the theory while the critical density is underestimated. Despite these differences the error seems to be systematic and it is gratifying to note that the general trends in the critical properties are reproduced by the present theory and model, including the anomolous behavior of methane in terms of the critical pressure. This is in agreement with the work of Boublík[14] and Vega and MacDowell[25] who have studied these trends in more detail.

Figure 7 shows the $T - \rho$ plots for the LV coexistence of the *n*-alkane systems and the fitted theoretical results. The results for hexane and heptane have been excluded for clarity; however, the fittings to these systems are of comparable accuracy to the other system. In all cases, away from the critical point, the LV coexistence envelopes are described in a satisfactory manner. For the reasons explained above the critical points are not reproduced. It is difficult to see how well the theory describes the coexisting vapor phase solely from the $T - \rho$ plots. For this reason the vapor volumes are presented in Figure 8. For the shorter alkanes the agreement between the theory and experiment is reasonably good; however, the results are less satisfactory for the longer alkanes. The fittings could, however,

be improved. In this work the fittings have been made using only the $T - \rho$ data for the alkanes. Thus, a small discrepancy in the vapor density will lead to a large deviation in the vapor volumes. Using the simplex method described in ref 3, it is possible to minimize the square of the difference between the experimental points and the theoretical predictions for the vapor volume data, the liquid densities, and the Clausius−Clapyeron data. The problem with these types of fittings is that they are far more time consuming than the simple method used for this work.

Overall, despite the simplicity of the model and fitting method, the SWSC seems to give a reasonable description of the LV phase behavior of the smaller members of the *n*-alkane series. As the alkane chains increase in length it is likely that effects of flexibility and the existence of different torsional conformations become more important. In these cases a more complex model is needed to describe the experimental data. However, for the shorter alkanes it may be possible to extend this theoretical description to explore the phase behavior of alkane mixtures.

5. Conclusions

A simple perturbation theory has been presented for a model fluid interaction through an SW potential of spherocylindrical shape. This PT describing this model was recently tested against simulation data for elongations of 5:1, and the description of the isotropic phase was found to be good. With this in mind the theory was used to explore the LV phase behavior of shorter spherocylinders. The theoretical results were compared to Gibbs Monte Carlo simulation data for the linear Kihara fluids. Interestingly enough, the effects of different molecular parameters on the phase behavior was found to be very similar for both models; however, the obvious advantage with the SWSC fluid is the exsistence of a good theoretical EOS with in which the SW range can be varied without extra computational difficulty.

The results from the theory were used to describe the thermodynamics of the *n*-alkane series, away from their critical points, with a good deal of success. It was interesting to note that despite the lack of numerical accuracy for the predictions of the alkane critical points, the deviations seemed to be systematic and all of the general trends were observed. We also reiterate that in this work the SWSC were considered as models for the thermodynamics of the *n*-alkanes series rather than molecular level models. Having said that, a systematic dependence of the fitting parameters was found with respect to the length of the alkane chain.

The theory may also be extended to included models in which ϵ, the SW well depth, is dependent on the orientation of the molecules. This may allow a more accurate description of real molecular fluids, compensating for the increase in attractive forces as the alkane chains increase in length.

The SWSC may also be used as a reference system to model polar fluids, in which the anisotropy in the shape of the molecule, as well as the electronic distribution, cannot be ignored. It may be possible to obtain a good description of carbon dioxide with such a model. The advantage with such a simple model would be the extension of the theory to examine mixtures of real polar fluids.

Acknowledgment. This work received support from CONACyT (4139P-E9608).

References and Notes

(1) Gray, C. G.; Gubbins, K. E. *Theory of Molecular Fluids*; Oxford: Clarendon, 1979; Vol. I.
(2) Vega, C.; Lago, S.; De Miguel, E.; Rull, L. F. *J. Phys. Chem.* **1992**, *105*, 2837.
(3) Gil-Villegas, A.; Galindo, A.; Whitehead, P. J.; Mills, S. J.; Jackson, G.; Burgess, A. N. *J. Chem. Phys.* **1997**, *106*, 4168.
(4) Garzon, B.; Lago, S.; Vega, C.; De Miguel E.; Rull, L. F. *J. Chem. Phys.* **1994**, *101*, 4166.
(5) Benavides, A. L.; Guevara, Y.; Del Rio, F. *Physica* **1994**, *A202*, 420.
(6) Del Rio, F.; Benavides, A. L.; Guevara, Y. *Physica* **1995**, *A215*, 10.
(7) Guevara, Y.; Benavides, A. L.; Del Rio, F. *Mol Phys.* **1996**, *88*, 10.
(8) Kihara, T. *Phys. Soc. Jpn.* **1951**, *16*, 289.
(9) Gay, J. G.; Berne, B. J. *J. Chem. Phys.* **1981**, *74*, 3316.
(10) Berne, B. J.; Pechukas, J. *J. Chem. Phys.* **1972**, *56*, 4213.
(11) Velasco, E.; Somoza, A. M.; Mederos *J. Chem. Phys.* **1995**, *102*, 8107.
(12) Boublík, T. *J. Chem. Phys.* **1975**, *87*, 1751.
(13) Vega, C.; Lago, S. *J. Chem. Phys.* **1991**, *94*, 310.
(14) Boublík, T. *Mol. Phys.* **1998**, *95*, 363.
(15) Williamson, D. C.; Del Rio, F. *J. Chem. Phys.* **1998**, *109*, 4675.
(16) Somoza, A. M.; Tarazona, P. *J. Chem. Phys.* **1989**, *91*, 517.
(17) Gil-Villegas, A.; Del Rio, F.; Benavides, A. L. *Fluid Phase Equilib.* **1996**, *119*, 97.
(18) Carnahan, N. F.; Starling, K. E. *J. Chem. Phys.* **1969**, *51*, 635.
(19) Lee, S. D. *J. Chem. Phys.* **1987**, *87*, 4972.
(20) Parsons, J. D. *Phys. Rev.* **1979**, *A19*, 1225.
(21) Guggenheim, E. A. *J. Chem. Phys.* **1945**, *13*, 253.
(22) Pitzer, K. S. *J. Am. Chem. Soc.* **1955**, *77*, 3427.
(23) Smith, B. D.; Srivastava, R. *Thermodynamic Data for Pure Compounds*; Elsevier: Amsterdam, 1986.
(24) Paulícek, J.; Aim, K.; Boublík, T. *J. Phys. Chem.* **1995**, *99*, 15662.
(25) Vega, C.; MacDowell, L. G. *Mol. Phys.* **1996**, *88*, 1575.